Hindawi Publishing Corporation
International Journal of Photoenergy
Volume 2013, Article ID 817424, 11 pages
http://dx.doi.org/10.1155/2013/817424

Research Article

Thin Film CIGS Solar Cells, Photovoltaic Modules, and the Problems of Modeling

Antonino Parisi, Luciano Curcio, Vincenzo Rocca, Salvatore Stivala, Alfonso C. Cino, Alessandro C. Busacca, Giovanni Cipriani, Diego La Cascia, Vincenzo Di Dio, Rosario Miceli, and Giuseppe Ricco Galluzzo

DEIM, University of Palermo, Viale delle Scienze, Building 9, 90128 Palermo, Italy

Correspondence should be addressed to Rosario Miceli; rosario.miceli@unipa.it

Received 13 July 2013; Accepted 13 August 2013

Academic Editor: Leonardo Palmisano

Copyright © 2013 Antonino Parisi et al. This is an open access article distributed under the Creative Commons Attribution License, which permits unrestricted use, distribution, and reproduction in any medium, provided the original work is properly cited.

Starting from the results regarding a nonvacuum technique to fabricate CIGS thin films for solar cells by means of single-step electrodeposition, we focus on the methodological problems of modeling at cell structure and photovoltaic module levels. As a matter of fact, electrodeposition is known as a practical alternative to costly vacuum-based technologies for semiconductor processing in the photovoltaic device sector, but it can lead to quite different structural and electrical properties. For this reason, a greater effort is required to ensure that the perspectives of the electrical engineer and the material scientist are given an opportunity for a closer comparison and a common language. Derived parameters from ongoing experiments have been used for simulation with the different approaches, in order to develop a set of tools which can be used to put together modeling both at single cell structure and complete module levels.

1. Introduction

Thin film solar cells based on a compound of the elements Copper, Indium, Gallium, and Selenium, that is, CIGS semiconductors, are considered as highly promising light-to-electricity converters thanks to their direct bandgaps which can be efficiently matched to the solar spectrum [1]. Among different fabrication methods suitable for the absorber layer, electrodeposition represents an important alternative to the expensive vacuum-based technologies. Using a single-step electrodeposition, several groups have fabricated CIGS films [2], and in some case an efficiency exceeding 15% has been reported [3], not too far from top performances made possible by the most studied vacuum-based three-stage process [1].

One of the most important requirements for successful application of the one-step electrodeposition here considered, for CIGS film production, is to control composition of deposited films in a reliable and reproducible way (it is noteworthy that we found several technological requirements in common with optical applications we had previously developed in different research contexts, to which we address the reader [4–19]).

Furthermore, film formation must be manufacturing friendly, possibly eliminating the selenization step, which is environmentally undesired due to the toxicity of Se.

In some recent works [20, 21], we described our first results on the option to fabricate CIGS-based solar cells directly using electrodeposited films by adjusting the concentration of the solution and eliminating the unwanted selenization step. Within the limits of the present discussion, it will be enough to mention that (1) electrodeposition of CIGS, with a controlled and reproducible Cu/(In +Ga) and Ga/(In +Ga) molar ratios, has been presented and (2) Cu-In-Se-Ga content and formation of secondary phases before and after the annealing process have been investigated [4, 6].

Also, in the context of our research project, it is required to derive parameters from ongoing experiments on the layered junction structures and use them for simulation with different approaches, in order to develop a set of tools which can be used to put together modeling both at single cell and module levels, what we will describe here. To complete the

overall picture of the ongoing activity, we will mention that we are adapting a previous sensor measurement setup to map solar cell performance with a light-beam-induced current (LBIC) configuration [22–24].

In particular, from real data, we have derived the five-parameter model and the complete characteristic of a CIGS module. Afterwards, from a structural model, setting real CIGS cells parameters, we have derived the cell characteristic. A circuital model—able to describe the cells interconnections and packaging—took into account the simulated cells data, has been finally compared with the previously mentioned module simulation. This comparison could be very useful to determine the internal parameters that extend the structural cells model to the module characteristics, so that the different perspectives of the electrical engineer and the material scientist are given an opportunity for a closer collaboration and a common language we are actively looking for [25].

Hence, this paper is organized as follows. In Section 2 we describe a general introduction to model simulation methods and the five-parameter analysis of a real CIGS module. Then, structural cell simulation is described in Section 3 together with a parasitic network resistance modeling and a comparison with the module data. Finally, conclusions are drawn in Section 4.

2. Five Lumped Parameters Simulation

A photovoltaic (PV) module mathematical model is a very useful tool to evaluate electrical energy production during the operative working of PV plants [26]. Moreover, such models are important to perform economic evaluations and compare different PV plants implementations [27–30].

In the literature, seldom parametric mathematical models have been proposed to simulate the solar cell functioning on the basis of distributed parameters equivalent circuits, while lumped parameters equivalent circuits are largely more common [31–35]. Among the lumped parameters models, there are different implementations that consider four, five, or six parameters with various threshold accuracies. Model parameters can be evaluated on the basis of the numerical data from the manufacturers [31–34, 36, 37]. Finally, fitting methods are used to match I-V characteristic curves with different temperature and irradiance values.

Among lumped parameters equivalent circuit models, the five-parameter one has been here taken into account. The lumped parameters single diode model (Figure 1), thanks to the shunt resistor (R_{sh}), is able to simulate, with good accuracy, the solar cell working condition. It is also able to work correctly even at low irradiance conditions and it shows a lower computational burden in comparison, for example, to the double diode model.

The five lumped cell parameters are described herein:

(i) the photoelectric current that depends on temperature, radiation, and structural characteristics (I_L);

(ii) the diode saturation current that depends on temperature and structural characteristics (I_0);

(iii) the diode quality factor that depends on the cell junction characteristics (γ);

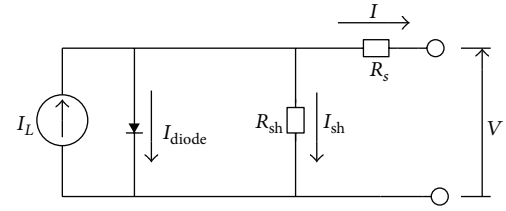

Figure 1: Five lumped parameters cell model.

(iv) the series resistance that depends on the structural characteristics of the cell (R_s);

(v) the shunt resistance that depends on the structural characteristics of the cell (R_{sh}).

The photocurrent depends on cell irradiance, temperature, and structural characteristics. Moreover, it is directly proportional to the irradiancy. The diode, in the equivalent circuit, represents the recombination current in the quasi-neutral region of the p-n junction [32, 38]. The standard Shockley equation for the circuit in Figure 1 is as follows:

$$I_{\text{diode}} = I_0 \left[e^{q((V+IR_s)/(k\gamma T_c))} - 1 \right], \tag{1}$$

where

(i) q is the electron charge [C],

(ii) T_c is the cell temperature [K],

(iii) k is the Boltzmann constant [J/K],

(iv) V is the cell output voltage [V],

(v) I is the cell output current [A].

The diode thermal voltage $\gamma(kT_c/q)$ is also indicated with V_t.

The series resistance R_s represent internal losses of different kind; more relevant are [39, 40]

(i) front and back electrode resistances;

(ii) lead resistance;

(iii) metal semiconductor ohmic contact.

The shunt resistance takes into account the overall photovoltaic cell dispersion currents.

Eventually, the analytic relation of the cell characteristic is

$$I = I_L - I_0 \left[e^{q((V+IR_s)/(k\gamma T_c))} - 1 \right] - \frac{V + IR_s}{R_{\text{sh}}}. \tag{2}$$

It is fortunate that the same model can be extended to represent even the photovoltaic module when identical cells—also at the same temperature and irradiation—are connected either in series or in parallel.

For example, for the series of two cells, using the five-parameter model, the equivalent circuit is that depicted in Figure 2 [41, 42].

Having the two cells identical, at the same temperature and irradiated at the same intensity, we obtain

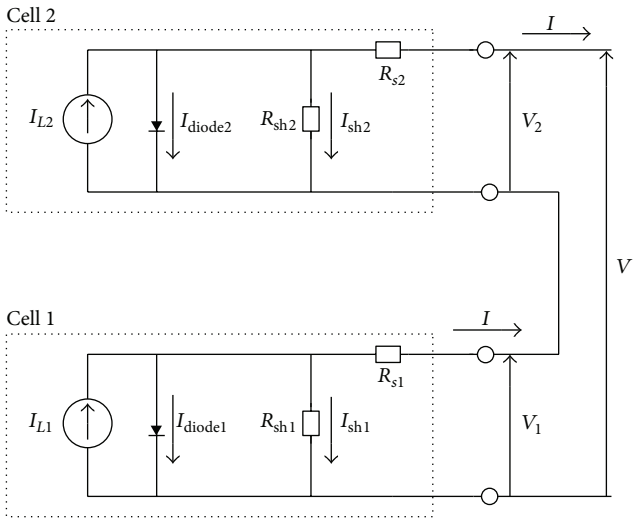

Figure 2: Equivalent circuit of the two cell series.

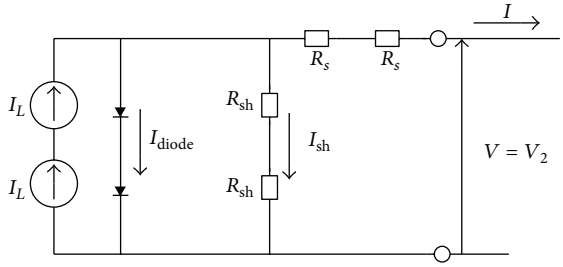

Figure 3: Equivalent circuit of a two identical cell series.

(i) $I_{L1} = I_{L2}$;

(ii) $V_1 = V_2$;

(iii) $I_{\text{diode1}} = I_{\text{diode2}}$ having the two identical diodes the same working conditions;

(iv) $R_{s1} = R_{s2}$;

(v) $R_{\text{sh1}} = R_{\text{sh2}}$;

(vi) $I_{\text{sh1}} = I_{\text{sh2}}$.

The aforementioned two cells scheme, in the previous hypothesis, is equivalent in the final analysis to the following simpler circuit of Figure 3 [41, 43, 44].

The extension to N_{CS} cells, connected in series, is obvious and the analytic relation for the module is then

$$I = I_L - I_0 \left[e^{q((V+IR_s)/k\gamma N_{\text{CS}} T_c)} - 1 \right] - \frac{V + IR_s}{R_{\text{sh}}}. \tag{3}$$

In order to evaluate the five-parameter values, the method hereafter reported has been adopted [33, 45, 46]. Equation (3) is written by the three characteristic points: maximum power, short-circuit, and open-circuit points, obtaining (4), (5), and (6), respectively. Moreover, the $dP/dV = 0$ condition by the maximum power point is derived, giving (7). Finally, the fifth equation is obtained by calculating the dI/dV value calculated in the short-circuit point, which results in (8). Equations (4) and (6) allow to evaluate I_0^{ref} (9). Equations (9) and (5) are developed to build (10), where the three unknowns R_s, R_{sh}, and V_t have to be evaluated. Equation (10) together with (7) and (8) allow to get (12) and (13). R_s, R_{sh} and V_t values are determined from (10), (12), and (13) through the iterative method hereafter reported:

$$I_{\text{SC}}^{\text{ref}} = I_L^{\text{ref}} - I_0^{\text{ref}} \cdot e^{(I_{\text{SC}}^{\text{ref}} R_s)/(N_{\text{CS}} V_t)} - \frac{I_{\text{SC}}^{\text{ref}} R_s}{R_{\text{sh}}}, \tag{4}$$

$$I_{\text{MP}}^{\text{ref}} = I_L^{\text{ref}} - I_0^{\text{ref}} \cdot e^{(V_{\text{MP}}^{\text{ref}} + I_{\text{MP}}^{\text{ref}} R_s)/(N_{\text{CS}} V_t)} - \frac{V_{\text{MP}}^{\text{ref}} + I_{\text{MP}}^{\text{ref}} R_s}{R_{\text{sh}}}, \tag{5}$$

$$I_L^{\text{ref}} - I_0^{\text{ref}} \cdot e^{(V_{\text{OC}}^{\text{ref}})/(N_{\text{CS}} V_t)} - \frac{V_{\text{OC}}^{\text{ref}}}{R_{\text{sh}}} = 0, \tag{6}$$

$$\left.\frac{dP}{dV}\right|_{V=V_{\text{MP}}^{\text{ref}}, I=I_{\text{MP}}^{\text{ref}}} = I_{\text{MP}}^{\text{ref}} + \left.\frac{dI}{dV}\right|_{V=V_{\text{MP}}^{\text{ref}}, I=I_{\text{MP}}^{\text{ref}}} V_{\text{MP}}^{\text{ref}} = 0, \tag{7}$$

$$\left.\frac{dI}{dV}\right|_{I=I_{\text{SC}}^{\text{ref}}} = -\frac{1}{R_{\text{sh}}}, \tag{8}$$

$$I_0^{\text{ref}} = \left(I_{\text{SC}}^{\text{ref}} - \frac{V_{\text{OC}}^{\text{ref}} - I_{\text{SC}}^{\text{ref}} R_s}{R_{\text{sh}}} \right) \cdot e^{-(V_{\text{OC}}^{\text{ref}})/(N_{\text{CS}} V_t)}, \tag{9}$$

$$I_{\text{MP}}^{\text{ref}} = I_{\text{SC}}^{\text{ref}} - \frac{V_{\text{MP}}^{\text{ref}} + I_{\text{MP}}^{\text{ref}} \cdot R_s - I_{\text{SC}}^{\text{ref}} \cdot R_s}{R_{\text{sh}}} - \left(I_{\text{SC}}^{\text{ref}} - \frac{V_{\text{OC}}^{\text{ref}} - I_{\text{SC}}^{\text{ref}} \cdot R_s}{R_{\text{sh}}} \right) K_T, \tag{10}$$

where

$$K_T = e^{(V_{\text{MP}}^{\text{ref}} + I_{\text{MP}}^{\text{ref}} R_s - V_{\text{OC}}^{\text{ref}})/(N_{\text{CS}} V_t)} \tag{11}$$

$$\left.\frac{dP}{dV}\right|_{V=V_{\text{MP}}^{\text{ref}}, I=I_{\text{MP}}^{\text{ref}}} = I_{\text{MP}}^{\text{ref}} + V_{\text{MP}}^{\text{ref}} \cdot \frac{-\dfrac{\left(I_{\text{SC}}^{\text{ref}} R_{\text{sh}} - V_{\text{OC}}^{\text{ref}} + I_{\text{SC}}^{\text{ref}} R_s\right) \cdot e^{(V_{\text{MP}}^{\text{ref}} + I_{\text{MP}}^{\text{ref}} R_s - V_{\text{OC}}^{\text{ref}})/(N_{\text{CS}} V_t)}}{N_{\text{CS}} V_t R_{\text{sh}}} - \dfrac{1}{R_{\text{sh}}}}{1 + \dfrac{\left(I_{\text{SC}}^{\text{ref}} R_{\text{sh}} - V_{\text{OC}}^{\text{ref}} + I_{\text{SC}}^{\text{ref}} R_s\right) \cdot e^{(V_{\text{MP}}^{\text{ref}} + I_{\text{MP}}^{\text{ref}} R_s - V_{\text{OC}}^{\text{ref}})/(N_{\text{CS}} V_t)}}{N_{\text{CS}} V_t R_{\text{sh}}} + \dfrac{R_s}{R_{\text{sh}}}} \tag{12}$$

$$-\frac{1}{R_{sh}}\Bigg|_{I=I_{SC}^{ref}} = \frac{-\dfrac{\left(I_{SC}^{ref}R_{sh}-V_{OC}^{ref}+I_{SC}^{ref}R_s\right)\cdot e^{(I_{SC}^{ref}R_s-V_{OC}^{ref})/(N_{CS}V_t)}}{N_{CS}V_tR_{sh}}-\dfrac{1}{R_{sh}}}{1+\dfrac{\left(I_{SC}^{ref}R_{sh}-V_{OC}^{ref}+I_{SC}^{ref}R_s\right)\cdot e^{(I_{SC}^{ref}R_s-V_{OC}^{ref})/(N_{CS}V_t)}}{N_{CS}V_tR_{sh}}+\dfrac{R_s}{R_{sh}}}. \quad (13)$$

In the equations detailed previously, standard test conditions, that is, STC, are indicate with "ref" as apex. To summarize the adopted iterative method, a block diagram is traced in Figure 4 [46].

At the first stage, the R_s and R_{sh} starting values are arbitrarily chosen and put into (10), in order to evaluate V_t. Subsequently, (13) is used to evaluate R_{sh}. The new R_{sh} value is put into (12) in order to check the $dP/dV = 0$ condition. If $dP/dV = 0$, the latter R_{sh} value is the right one and (2) can be used to evaluate the γ form factor; otherwise, the R_{sh} initial value has to be changed and the iteration goes on. The previously mentioned equations can be adopted in that form only under standard conditions. For this reason, it is necessary to take into account the changes of the I_0, I_L, I_{SC}, and V_{OC} parameters with respect to temperature and irradiation. According to [46, 47],

(i) I_0 does not depend on irradiation but only on temperature;

(ii) I_L depends only on temperature;

(iii) I_{SC} depends both on temperature and irradiation;

(iv) V_{OC} depends only on irradiation.

The following equations describe what was stated previously:

$$I_0(T) = \left(I_{SC}(T) - \frac{V_{OC}(T) - I_{SC}(T)R_s}{R_{sh}}\right)\cdot e^{-V_{OC}(T)/(N_{CS}V_t)}, \quad (14)$$

$$V_{OC}(T) = V_{OC}^{ref} + \mu_{V_{OC}}\left(T_C - T_C^{ref}\right), \quad (15)$$

$$I_{SC}(T) = I_{SC}^{ref}\left[1 + \frac{\mu_{I_{SC}}}{100}\left(T_C - T_C^{ref}\right)\right], \quad (16)$$

$$I_{SC}(G) = I_{SC}^{ref}\cdot\frac{G}{G^{ref}}, \quad (17)$$

$$I_L(G) = I_L^{ref}\cdot\frac{G}{G^{ref}}, \quad (18)$$

$$I_L(G,T) = \frac{G}{G^{ref}}\cdot\left[I_0(T)\cdot e^{V_{OC}(T)/(N_{CS}V_t)} + \frac{V_{OC}(T)}{R_{sh}}\right], \quad (19)$$

$$I_{SC}(G,T) = \frac{G}{G^{ref}}\cdot I_{SC}(T) = \frac{G}{G^{ref}}\cdot I_{SC}^{ref}\left[1 + \frac{\mu_{I_{SC}}}{100}\left(T_C - T_C^{ref}\right)\right], \quad (20)$$

where

(i) $\mu_{I_{SC}}$ is the short-circuit current temperature coefficient;

(ii) $\mu_{V_{OC}}$ is the open-circuit voltage temperature coefficient.

Therefore, (14), (15), (19), and (20) represent the five-parameter mathematical model under changing temperature and radiation conditions. Finally, the PV module output voltage can be expressed to good purpose by (21), derived from (1):

$$V = \left[\ln\left(\frac{I_L - I}{I_0} + 1 - \frac{V + IR_s}{I_0R_{sh}}\right)\right]N_{CS}V_t - IR_s. \quad (21)$$

For example, considering a commercial module with the following nominal data:

(i) $I_{SC} = 6.50$ A,

(ii) $V_{OC} = 46.8$ V,

(iii) $I_{MP} = 5.70$ A,

(iv) $V_{MP} = 34.4$ V,

(v) $\mu_{I_{SC}} = -0.03\%/\text{K}$,

(vi) $\mu_{V_{OC}} = -0.33\%/\text{K}$,

the resulting five lumped parameter values are:

(i) $\gamma = 1.5$,

(ii) $R_s = 0.94\,\Omega$,

(iii) $R_{sh} = 120\,\Omega$,

(iv) $I_L = 6.6$ A,

(v) $I_0 = 3.7\cdot10^{-7}$ A.

In the following picture (Figure 5), the behavior of the commercial module characteristic obtained from the five-parameter model in depicted, which will be used later on for a paired comparison.

3. The Structural Model from the Cell to the Module

In parallel to the previously described approach, usually the first choice for the electrical engineer, it is worthwhile to follow as well the microscopic point of view, more familiar to the material scientist. In order to generate a current, energy derived from the sun must impact on a photovoltaic device having a preexisting electrical field such that free electrons can succeed in separating from holes. Nowadays, numerical simulation offers advantages to the design, performance prediction, and comprehension of the fundamental phenomena ruling the operation of complex devices, such as solar cells, also allowing to investigate the physics of their inner processes.

Our tool of choice was wxAMPS, a software capable of representing the electrical transport phenomena and the optical response of a wide variety of layered structures like

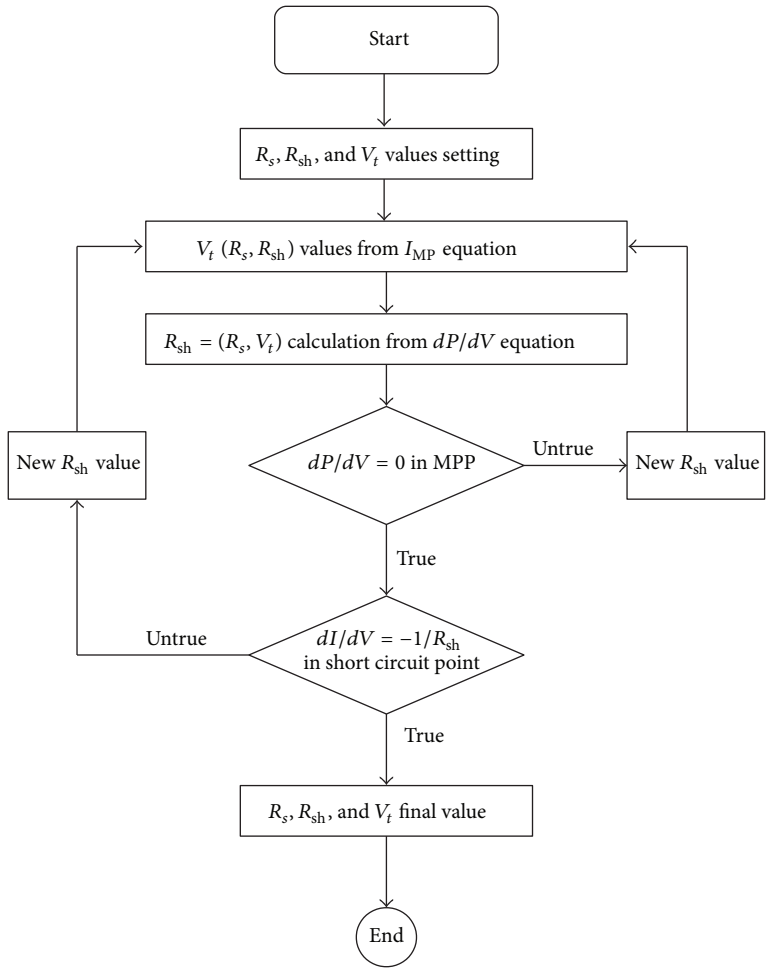

Figure 4: Determination of R_s, R_{sh}, and V_t: block diagram.

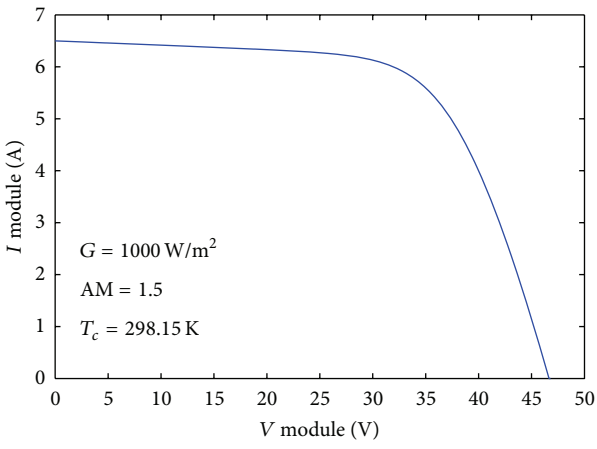

Figure 5: I-V curve from the five-parameter model of a commercial PV module.

those typical of solar cells. For this reason, it was also applied to simulate the behavior of the solar cell discussed in this work. This software is an updated version, rewritten in C++, of the one-dimensional simulation program Analysis of Microelectronic and Photonic Structures (AMPS-1D) that was initially developed by Fonash et al. at Pennsylvania State University [48, 49]. Various layers of stacked materials, producing homojunctions, heterojunctions, and multijunctions, can be studied by appropriately selecting characteristic parameters.

Thus, wxAMPS is a modern, often updated, solar cell simulator for modeling one-dimensional devices composed of several materials. It accepts the same input parameters as AMPS and is based on similar physical principles and numerical descriptions of defects and recombinations [49], while adding tunnelling effects based on trap-assisted and intraband tunnelling models [50, 51]. This program incorporates a new algorithm combining the Gummel and Newton methods. In fact, Gummel's method alone is of limited usefulness when simulating devices with very high defect densities, while Newton's method alone works poorly when determining intraband tunnelling current. The advantages of the combination are in terms of better stability and more consistent convergence in problems in which intraband

tunnelling is critical in the determination of precise solutions [52].

With wxAMPS, a hypothetically unlimited number of layers can be modeled; this added flexibility is suited to tailoring designs of devices with parameters, at any given depth profile, so as to establish optimal degrees of efficiency conversions for solar cells. The program allows data input through three main windows that represent the ambient conditions, the properties of different materials for the individual layers, and the resolving model (trap-assisted tunnelling or intraband). You can use the simulation parameters provided by the University of Illinois, Engineering Wiki [53], or you can set custom data as needed. Operating temperature, solar spectrum, quantum efficiency, front and back contact data, surface recombination velocity, and bias voltages are the environmental parameters which set device working conditions. Once stored, ambient conditions are defined for environment simulation, but new settings can be edited by users loading a properly tailored file. In detail, it is possible to take into account the values of Φ_B (the barrier height defined as $E_c - E_f$) for the front and back contacts and reflection coefficients [54].

The material properties of each layer are divided into four groups accessed by separate tabs: electrical, defect, optical, and advanced. A grid allows users to control and edit the overall structure of the device. Tables organize material properties and these are provided by a Wiki [53] website or are editable using common worksheets. Likewise, absorption coefficients can be edited directly by users or be loaded from external data files.

Once all required input is entered, it is possible to start data analysis. The results are displayed by an efficient graphical layout that presents them. Output data can be provided in two main forms: directly through the graphical user interface or indirectly through files readable by common spreadsheet programs.

A CIGS thin film solar cell structure, with parameters derived from our experiments, was simulated after specifying, as the input data, the material parameters for each individual layer of the stacked device structures. Specifically, several layers including the top contact, bottom contact, intrinsic ZnO layer, CdS buffer layer, high-recombination interface, surface defect layer on top of the CIGS film, and CIGS absorber defined the CIGS solar-cell structure. The employed thicknesses of structural layers and the material parameters, which by the way fall into the acceptable ranges reported in the literature [55], are shown in Table 1.

As usual, room temperature and standard sunlight (AM 1.5 G) were the assumed working conditions. Furthermore, the material parameters used in the simulations were kept unchanged. Tables 2 and 3 summarize material Gaussian defect states and contact parameters, respectively; Table 4 provides an explanation of the symbols used in the previous tables. The front and back contacts are solely defined by their work functions Φ_B.

Considering that an accurate optical assessment of a photovoltaic cell is hardly trivial, in order to facilitate the discussion and describe the considered simplifications, we will try to follow and illustrate reflections and absorptions to which photons from incident sunlight impacting on cells are exposed in their path.

As illustrated in Figure 6, incident rays reflect at the air-glass (1), glass-encapsulant (3), and encapsulant-cell (5) interfaces. In the latter case, reflection is often diffuse, leading

Table 1: Simulation material parameters of the CIGS thin-film solar cell.

Parameter	ZnO : Al	ZnO	CdS	CIGS
d (μm)	0.5	0.2	0.05	3
ε_R	9	9	10	13.6
E_g (eV)	3.3	3.3	2.4	1.18
χ (eV)	4.4	4.4	4.2	4.5
N_C [cm^{-3}]	$2.2 \cdot 10^{18}$	$2.2 \cdot 10^{18}$	$2.2 \cdot 10^{18}$	$2.2 \cdot 10^{18}$
N_V [cm^{-3}]	$1.8 \cdot 10^{19}$	$1.8 \cdot 10^{19}$	$1.8 \cdot 10^{19}$	$1.8 \cdot 10^{19}$
μ_n [cm^2/(V·s)]	100	100	100	100
μ_p [cm^2/(V·s)]	25	25	25	25
N_D [cm^{-3}]	$1 \cdot 10^{18}$	$1 \cdot 10^{7}$	$1.1 \cdot 10^{18}$	0
N_A [cm^{-3}]	0	0	0	$2 \cdot 10^{16}$

Table 2: Simulation material Gaussian defect for the CIGS solar layers.

Parameter	ZnO : Al	ZnO	CdS	CIGS
Defect type	Donor	Donor	Acceptor	Donor
Energy level [eV]	1.65	1.65	1.2	0.6
Deviation [eV]	0.1	0.1	0.1	0.1
σ_n [cm^2]	1×10^{-12}	1×10^{-12}	1×10^{-17}	5×10^{-13}
σ_p [cm^2]	1×10^{-15}	1×10^{-15}	1×10^{-12}	1×10^{-15}
N_t [cm^{-3}]	1×10^{17}	1×10^{17}	1×10^{18}	1×10^{14}

Table 3: Contact parameters applied to the simulations.

Parameter	Back contact	Front contact
ϕ_B [eV]	0.66	0
S_n [cm/s]	2×10^{7}	1×10^{7}
S_p [cm/s]	2×10^{7}	1×10^{7}

Table 4: Explanation of the symbols used to describe the simulation parameters.

Parameter	Explanation
D	Layer thickness
ε_R	Permittivity constant
χ	Electron affinity
N_C/N_V	Effective density of states in the conduction /valence band
μ_n/μ_n	Mobility of electrons/holes
σ_n/σ_p	Capture cross-section of electrons/holes
N_D/N_A	Doping concentration
N_t	Defect concentration
ϕ_B	Potential barrier height
S_n/S_p	Surface recombination velocity of electrons/holes

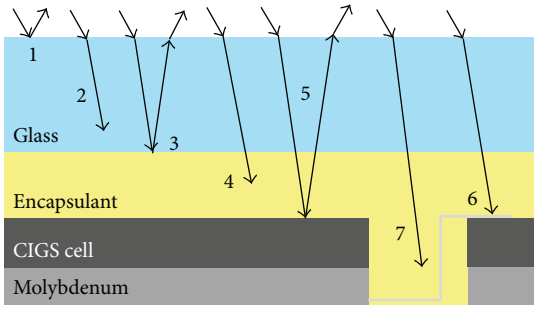

Figure 6: Cross-sectional diagram of a conventional photovoltaic module (not in scale), and the optical loss as described in the text.

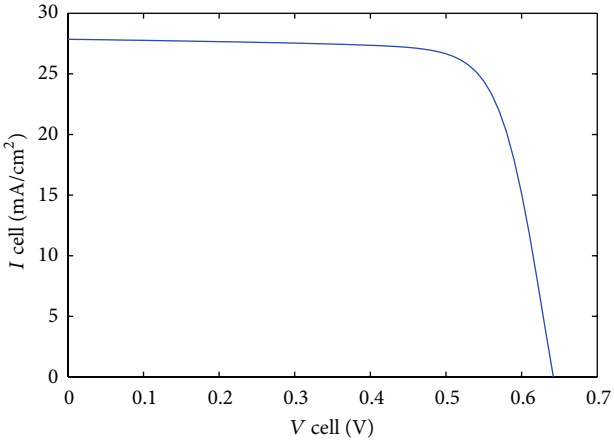

Figure 7: I-V curve (per cm^2) a simulated CIGS solar cell.

to some of the reflected light being totally internally reflected at the glass-air interface, remaining within the cell.

Furthermore, incident rays are absorbed by the glass (2), the encapsulant (4), and the cell's antireflection coating or metal fingers (6). In addition, further losses arise from incident rays within interspace between adjacent cells (7).

These seven interactions depend on the light's incident wavelength and angle [56].

In order to take into account overall losses due to reflection and absorption, we have set to 0.2 the reflection coefficient for light impinging on the uppermost surface. Instead, for the back surface, the reflection coefficient was set to 0.9.

As well known, a CIGS solar cell presents a composite structure and the study is difficult due to this stratified window, consisting of a thin Al doped ZnO layer, an un-doped ZnO, a CdS buffer layer (or using Cd-free buffer layers). In order to predict the behavior of solar cells with a complex structure, as in the case in analysis, it is important to use specific and detailed physical models which are implemented to the computer, so that the effect of considered input material parameters can be defined and assessed quantitatively.

Figure 7 shows the I-V characteristic (per cm^2), calculated using wxAMPS again, of the CIGS solar cell structure having material parameters listed in Tables 1–4, at room temperature and standard sunlight (AM 1.5 G).

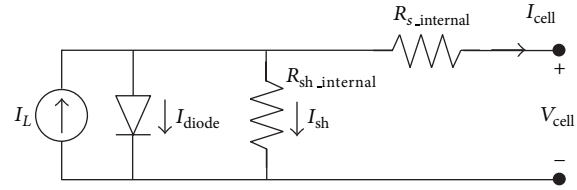

Figure 8: The one diode model for a p-n-junction solar cell.

Now, we will recall a brief qualitative description of the I-V characteristic curve of a common solar cell. In fact, a normal I-V curve presents a smooth shape in which it is possible to distinguish three distinct voltage regions: first, above 0 V, a slightly sloped region; second, below V_{OC}, a steeply sloped and, in the region of the maximum power point, a "knee." As shown in Figure 7, normally the three regions are smooth and continuous, but the position of the knee depends on cell technology and manufacturer. In detail, crystalline silicon cells show sharper knees whereas thin film solar cells have gradual knees. The slopes of the curve in the first two regions are caused by parasitic effects.

Truth be told, several causes lead to the power dissipation in solar cells, but among these the most important is power dissipation due to parasitic resistances. Figure 8 represents the one diode equivalent circuit for a p-n-junction solar cell and, in this model, solar cells are described as a current generator in parallel with a diode and a shunt resistance, internal R_{sh} of cell which all are connected in series with another resistance, internal R_s of cell. I_L is the photogenerated current and I_{diode} is the current within a p-n-junction solar cell diode whereas I_{sh} and I_{cell} are the currents into parasitic resistances (i.e., internal R_{sh} and R_s). In order to design a performing solar cell, internal R_s should be as low as possible and R_{sh} as high as possible.

For a typical CIGS cell, formation of internal series resistance (R_s) of the cell, is mainly due to a ZnO:Al layer film resistance (typically 15 Ω/□), resistances of various cell layers, and resistance of top and back contacts. In particular, the contact resistance between CIGS absorber layer and Molybdenum (back contact) can be ohmic or junction-like depending on type and CIGS doping level.

It is assumable that in a common solar cell, R_{sh} arises from current leaking within the cell in high-conducting paths cross the p-n-junction or around the edges. Shunt paths, that is, high-conducting paths, within the material can be a result of presence of the impurities or crystal damage during the production phases [57].

The simulation program wxAmps takes into account overall volume resistances and the two resistances of back and top contact that arise in different device layers. In particular, Figure 7 shows I-V curve obtained from simulations with wxAmps. This curve shows that the simulated cell has an internal series resistance equal to 1.8 [$\Omega \times$ cm^2] and an internal shunt resistance equal to 890 [$\Omega \times$ cm^2], respectively.

In order to determine the electrical behaviour of the module, starting from individual cells, other resistive contributions to those simply derivable from I-V characteristic of

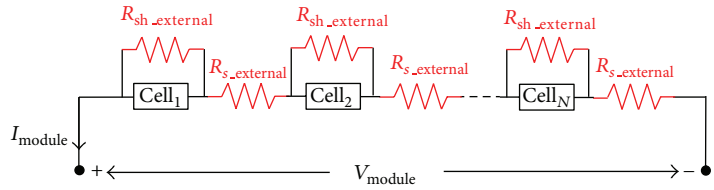

Figure 9: Equivalent electrical scheme of module.

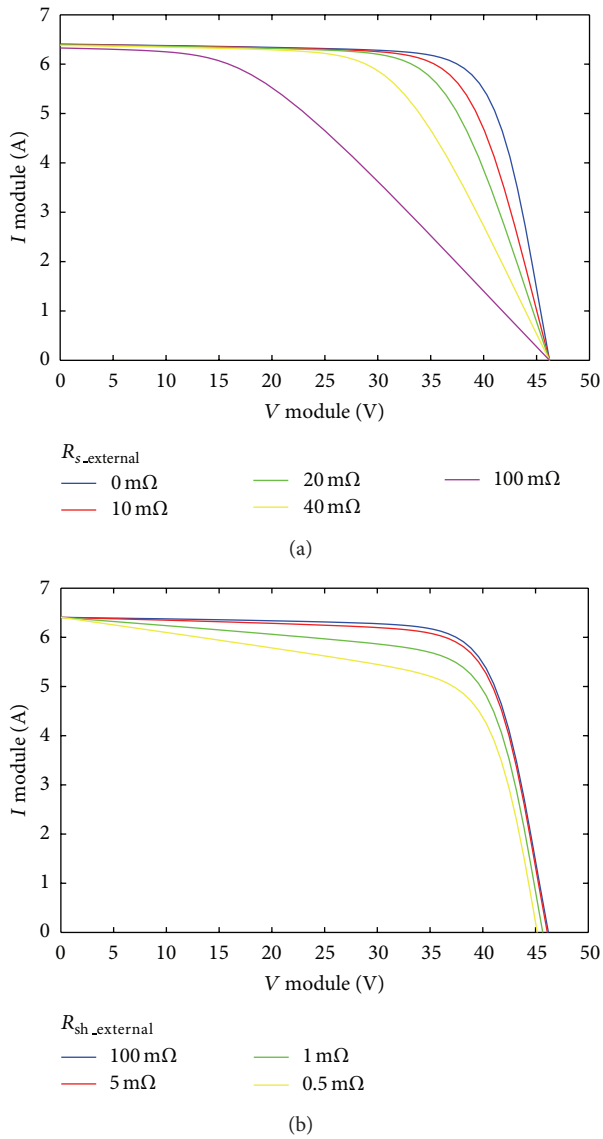

Figure 10: Effects of parasitic resistance on the simulated I-V characteristics of 230 cm^2 CIGS solar cell. (a) Increasing external series resistance. (b) Increasing external shunt resistance.

elementary cell must be added: sheet resistance of ZnO:Al, grid contributions, and interconnection resistance between module cells (i.e., metallic interconnections and contacts) [58].

Such contributions shall be considered separately because wxAmps is a one-dimensional simulator and device's cross-sectional dimensions and interconnections between cells are neglected. Similarly, we must also consider additional shunt resistance of overall module mainly due to the fact that shunt paths exist in photovoltaic solar cell interconnects and module I_{sc} mismatch.

In detail, this additional shunt resistance is due to defects in materials or degradation of interconnections between cells monolithically integrated in a module. Dielectric material inhomogeneities and defects in thin-film solar cells or crystal damage that can produce a variation of the shunt resistance, extending to cells (shunt currents through the p-n junction), have been observed experimentally [59]. Unintentional partial shorting of cell near edges can cause a highly ohmic shunt path, for example, connection between front-front and the back-back contacts of all cells. Shunt currents between the front and back contacts of cells are other possible causes.

The set of all these additional resistances are simplified considering electrical model of Figure 9 obtained adding the resistors $R_{sh_external}$ and $R_{s_external}$. The electric model was properly evaluated to switch from single cell to complete module. The module considered in our study consists of 72 cells in series and each having an area of around 230 cm^2.

This step complicates the discussion by introducing (as we have seen) a network of parasitic resistances.

If $R_{sh_external}$ and $R_{s_external}$ are taken into account, according to scheme in Figure 9, I-V, equation of module can be written as a function of single cell:

$$I_{mod} = \frac{R_{sh_external} * I_{cell}}{R_{sh_external} + (R_{sh_external}/2)} - \frac{V_{mod}/N}{R_{sh_{external}} + (R_{sh_{external}}/2)}. \quad (22)$$

$R_{s_external}$ and $R_{sh_external}$ are detrimental to solar cell and module performance, in fact, both reduce fill factor as is illustrated in Figures 10(a) and 10(b).

The current I_{sh} leaking through the R_{sh} of module decreases current output, I_{module}, to intended load. The smaller R_{sh}, the greater I_{sh}, and lower I_{module} for a given voltage, V. A very low R_{sh} reduces V_{OC} but does not affect I_{sh}. R_s gives rise to a potential drop, which reduces the voltage output, V, but leaves V_{OC} unaffected, whereas a very high R_s reduces I_{SC}.

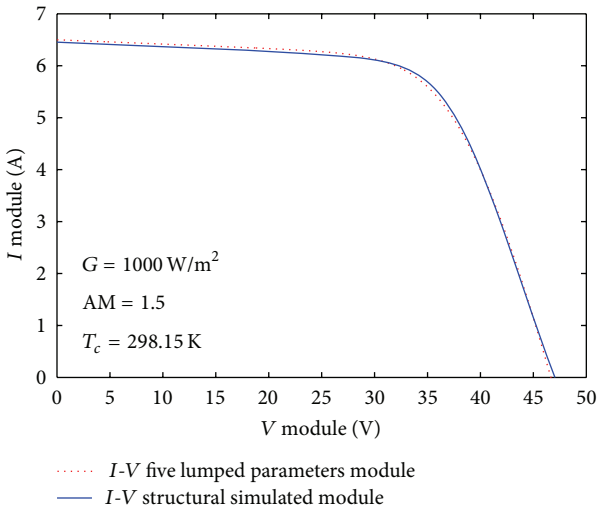

Figure 11: I-V curve from the five parameter model and structural model with parasitic resistances.

4. Comparison of Models and Conclusions

From the comparison of the five lumped parameters and the structural model of a PV commercial module, we have extracted the values of the local parasitic network resistances to be associated with the structural simulation. Figure 11 shows the good agreement which can be obtained between the two models.

Further refinements are required, but we think that the approach and methods here described can lead to the development of an important tool to evaluate intermediate results during CIGS cell technology development and assessment of its impact on global electrical module performance.

This is particularly useful in the course of a research activity which encompasses a variety of contributions from technical subjects such as electrochemistry, semiconductor science, electrical and electronic engineering, and optical measurements. We are trying to keep as linked as possible, during the task of modeling, both the level of single cell structure and that of the complete photovoltaic module. In other words, it is our way to look actively for a common language, so that the different perspectives of the electrical engineer and the material scientist are given an opportunity for a closer collaboration.

We are currently applying this approach to the fabrication of thin film CIGS solar cells by means of single-step electrodeposition, a technique which appears fairly easy and low cost but, at the same time, can lead to quite different structural and electrical properties, so that a reasonable estimation of its impact on module characteristics is required in all the intermediate steps of our project.

Conflict of Interests

Professor Rosario Miceli, declares the following: "MATLAB" and "SIMULINK" are registered trademarks of The MathWorks, Inc. "wxAMPS" is a freeware software made available by the University of Illinois at Urbana-Champaign (UIUC), in collaboration with Nankai University of China. In both cases all the authors do not have any conflict of interests with the content of the paper.

Acknowledgments

The activity described previously has been supported by the PON 01_1725 "Nuove tecnologie fotovoltaiche per sistemi intelligenti integrati in Edifici" and the PON 02_00355 "Tecnologie per l'ENERGia e l'Efficienza energETICa—ENERGETIC" Research Programs. Contributions came also from SDESLab University of Palermo. Finally, the authors express their gratitude to Professor Rockett, Yiming Liu, and Professor Fonash for making freely available their simulation software wxAMPS.

References

[1] T. Unold and C. A. Kaufmann, "1.18-chalcopyrite thin-film materials and solar cells," in *Comprehensive Renewable Energy*, E. C. A. Sayigh, Ed., pp. 399–422, Elsevier, Oxford, UK, 2012.

[2] V. S. Saji, I.-H. Choi, and C.-W. Lee, "Progress in electrodeposited absorber layer for $CuIn_{1-x}Ga_xSe_2$ (CIGS) solar cells," *Solar Energy*, vol. 85, no. 11, pp. 2666–2678, 2011.

[3] R. N. Bhattacharya, W. Batchelor, J. F. Hiltner, and J. R. Sites, "Thin-film $CuIn_{1-x}Ga_xSe_2$ photovoltaic cells from solution-based precursor layers," *Applied Physics Letters*, vol. 75, no. 10, pp. 1431–1433, 1999.

[4] A. C. Busacca, A. C. Cino, S. Riva-Sanseverino, M. Ravaro, and G. Assanto, "Silica masks for improved surface poling of lithium niobate," *Electronics Letters*, vol. 41, no. 2, pp. 92–94, 2005.

[5] A. C. Busacca, E. D'Asaro, A. Pasquazi, S. Stivala, and G. Assanto, "Ultraviolet generation in periodically poled lithium tantalate waveguides," *Applied Physics Letters*, vol. 93, no. 12, Article ID 121117, 2008.

[6] A. C. Busacca, C. A. Santini, S. R. Sanseverino et al., "Surface periodic poling in congruent lithium tantalate," *Electronics Letters*, vol. 42, no. 9, pp. 546–547, 2006.

[7] A. C. Busacca, C. L. Sones, R. W. Eason, and S. Mailis, "First-order quasi-phase-matched blue light generation in surface-poled Ti:indiffused lithium niobate waveguides," *Applied Physics Letters*, vol. 84, no. 22, pp. 4430–4432, 2004.

[8] A. C. Busacca, S. Stivala, L. Curcio, and G. Assanto, "Parametric conversion in micrometer and submicrometer structured ferroelectric crystals by surface poling," *International Journal of Optics*, vol. 2012, Article ID 606892, 11 pages, 2012.

[9] A. C. Busacca, S. Stivala, L. Curcio, and P. Livreri, "Random quasi-phase matching in congruent lithium tantalate waveguides by proton exchange," *Electronics Letters*, vol. 48, pp. 783–784, 2012.

[10] E. Cantelar, M. Domenech, G. Lifante et al., "Multi-line NIR-RGB emission in $Nd:LiNbO_3$ RPE optical waveguides," *Electronics Letters*, vol. 43, no. 11, pp. 632–633, 2007.

[11] E. Cantelar, G. Lifante, F. Cussó et al., "Dual-polarization-pump CW laser operation in $Nd^{3+}:LiNbO_3$ channel waveguides fabricated by reverse proton exchange," *Optical Materials*, vol. 30, no. 7, pp. 1039–1043, 2008.

[12] M. Cherchi, S. Bivona, A. C. Cino, A. C. Busacca, and R. L. Oliveri, "Universal charts for optical difference frequency

generation in the terahertz domain," *IEEE Journal of Quantum Electronics*, vol. 46, no. 6, pp. 1009–1013, 2010.

[13] M. Cherchi, S. Stivala, A. Pasquazi et al., "Second-harmonic generation in surface periodically poled lithium niobate waveguides: on the role of multiphoton absorption," *Applied Physics B*, vol. 93, no. 2-3, pp. 559–565, 2008.

[14] M. Cherchi, A. Taormina, A. C. Busacca et al., "Exploiting the optical quadratic nonlinearity of zinc-blende semiconductors for guided-wave terahertz generation: a material comparison," *IEEE Journal of Quantum Electronics*, vol. 46, no. 3, pp. 368–376, 2010.

[15] M. Clerici, L. Caspani, E. Rubino et al., "Counterpropagating frequency mixing with terahertz waves in diamond," *Optics Letters*, vol. 38, pp. 178–180, 2013.

[16] G. Nava, P. Minzioni, I. Cristiani et al., "Integrated frequency shifter in periodically poled lithium tantalate waveguide," *Electronics Letters*, vol. 46, no. 25, pp. 1686–1688, 2010.

[17] A. Pasquazi, A. Busacca, S. Stivala, R. Morandotti, and G. Assanto, "Nonlinear disorder mapping through three-wave mixing," *IEEE Photonics Journal*, vol. 2, no. 1, 2010.

[18] E. M. Rodríguez, D. Jaque, E. Cantelar et al., "Time resolved confocal luminescence investigations on Reverse Proton Exchange Nd:$LiNbO_3$ channel waveguides," *Optics Express*, vol. 15, no. 14, pp. 8805–8811, 2007.

[19] S. Stivala, A. Pazquazi, L. Colace et al., "Guided-wave frequency doubling in surface periodically poled lithium niobate: competing effects," *Journal of the Optical Society of America B*, vol. 24, no. 7, pp. 1564–1570, 2007.

[20] R. Inguanta, S. Piazza, C. Sunseri et al., "An electrochemical route towards the fabrication of nanostructured semiconductor solar cells," in *Proceedings of the International Symposium on Power Electronics, Electrical Drives, Automation and Motion (SPEEDAM '10)*, pp. 1166–1171, June 2010.

[21] R. L. Oliveri, R. Inguanta, T. Spanò et al., "CIGS thin film by one-step electrodeposition for solar cells," in *Proceedings of 15th Italian National Conference of Photonic Technologies (Fotonica '13)*, Milan, Italy, 2013.

[22] A. Parisi, A. C. Cino, A. C. Busacca, M. Cherchi, and S. Riva-Sanseverino, "Integrated optic surface plasmon resonance measurements in a borosilicate glass substrate," *Sensors*, vol. 8, no. 11, pp. 7113–7124, 2008.

[23] A. Parisi, F. P. D'Aleo, S. Guarino et al., "Integrated optic surface plasmon resonance measurements in glass substrates," in *Proceedings of the 3rd European Workshop on Optical Fibre Sensors*, vol. 6619 of *Proceedings of SPIE*, Napoli, Italy, July 2007.

[24] S. Stivala, A. Pasquazi, A. C. Busacca et al., "Frequency doubling in surface periodically poled lithium niobate waveguides: competing effects," in *Proceedings of the European Conference on Lasers and Electro-Optics and the International Quantum Electronics Conference (CLEOE-IQEC '07)*, Munich, Germany, 2007.

[25] A. Parisi, L. Curcio, V. Rocca et al., "Photovoltaic module characteristics from CIGS solar cell modelling," in *Proceedings of the International Conference Renewable Energy Research and Applications (ICRERA '13)*, 2013.

[26] R. Miceli, "Energy management and smart grids," *Energies*, vol. 6, pp. 2262–2290, 2013.

[27] G. Cipriani, V. Di Dio, D. La Manna, F. Massaro, R. Miceli, and G. Zizzo, "Economic analysis on dynamic photovoltaic systems in new italian "feed in tariffs" context," in *Proceedings of the International Conference on Clean Electrical Power: Renewable Energy Resources Impact (ICCEP'13)*, 2013.

[28] G. Cipriani, V. Di Dio, L. P. Di Noia et al., "A PV plant simulator for testing MPPT techniques," in *Proceedings of the International Conference on Clean Electrical Power: Renewable Energy Resources Impact (ICCEP '13)*, 2013.

[29] V. Di Dio, S. Favuzza, D. La Caseia, and R. Miceli, "Economical incentives and systems of certification for the production of electrical energy from renewable energy resources," in *Proceedings of the International Conference on Clean Electrical Power (ICCEP '07)*, pp. 277–282, May 2007.

[30] V. Di Dio, R. Miceli, C. Rando, and G. Zizzo, "Dynamics photovoltaic generators: technical aspects and economical valuation," in *Proceedings of the International Symposium on Power Electronics, Electrical Drives, Automation and Motion (SPEEDAM '10)*, pp. 635–640, June 2010.

[31] M. Bouzguenda, T. Salmi, A. Gastli, and A. Masmoudi, "Evaluating solar photovoltaic system performance using MATLAB," in *Proceedings of the 1st International Conference on Renewable Energies and Vehicular Technology (REVET '12)*, pp. 55—559.

[32] A. N. Celik and N. Acikgoz, "Modelling and experimental verification of the operating current of mono-crystalline photovoltaic modules using four- and five-parameter models," *Applied Energy*, vol. 84, no. 1, pp. 1–15, 2007.

[33] G. Cipriani, V. Di Dio, D. La Cascia, R. Miceli, and R. Rizzo, "A novel approach for parameters determination in four lumped PV parametric model with operative range evaluations," *International Review of Electrical Engineering*, vol. 8, 2013.

[34] G. Farivar and B. Asaei, "Photovoltaic module single diode model parameters extraction based on manufacturer datasheet parameters," in *Proceedings of the IEEE International Conference on Power and Energy (PECon '10)*, pp. 929–934, December 2010.

[35] M. G. Villalva, J. R. Gazoli, and E. R. Filho, "Comprehensive approach to modeling and simulation of photovoltaic arrays," *IEEE Transactions on Power Electronics*, vol. 24, no. 5, pp. 1198–1208, 2009.

[36] G. Cipriani, G. Ciulla, V. Di Dio, D. La Cascia, and R. Miceli, "A device for PV modules I-V characteristic detection," in *Proceedings of the International Conference on Clean Electrical Power: Renewable Energy Resources Impact (ICCEP '13)*, 2013.

[37] V. Lo Brano, A. Orioli, G. Ciulla, and A. Di Gangi, "An improved five-parameter model for photovoltaic modules," *Solar Energy Materials and Solar Cells*, vol. 94, no. 8, pp. 1358–1370, 2010.

[38] A. Luque and S. Egedus, *Handbook of Photovoltaic Science and Engineering*, Wiley, Chichester, UK, 2003.

[39] F. Ghani, M. Duke, and J. Carson, "Numerical calculation of series and shunt resistance of a photovoltaic cell using the Lambert W-function: experimental evaluation," *Solar Energy*, vol. 87, pp. 246–253, 2013.

[40] M. A. Green, *Solar Cells: Operating Principles, Technology, and System Applications*, vol. 1, Prentice Hall, Upper Saddle River, NJ, USA, 1982.

[41] A. Chatterjee, A. Keyhani, and D. Kapoor, "Identification of photovoltaic source models," *IEEE Transactions on Energy Conversion*, vol. 26, no. 3, pp. 883–889, 2011.

[42] S. Li and H. Zheng, "Energy extraction characteristic study of solar photovoltaic cells and modules," in *Proceedings of the IEEE Power and Energy Society General Meeting: The Electrification of Transportation and the Grid of the Future*, San Diego, Calif, USA, July 2011.

[43] H. -L. Tsai, C. S. Tu, and Y. J. Su, "Development of generalized photovoltaic model using MATLAB/SIMULINK," in *Proceedings of the World Congress on Engineering and Computer Science WCECS ('08)*, San Francisco, Calif, USA, 2008.

[44] M. G. Villalva, J. R. Gazoli, and E. Ruppert Filho, "Modeling and circuit-based simulation of photovoltaic arrays," in *Proceedings of the Brazilian Power Electronics Conference (COBEP '09)*, pp. 1244–1254, Bonito-Mato Grosso do Sul, Brazil, October 2009.

[45] W. De Soto, S. A. Klein, and W. A. Beckman, "Improvement and validation of a model for photovoltaic array performance," *Solar Energy*, vol. 80, no. 1, pp. 78–88, 2006.

[46] D. Sera, R. Teodorescu, and P. Rodriguez, "PV panel model based on datasheet values," in *Proceedings of the IEEE International Symposium on Industrial Electronics (ISIE '07)*, pp. 2392–2396, Vigo, Spain, June 2007.

[47] V. Di Dio, D. La Cascia, R. Miceli, and C. Rando, "A mathematical model to determine the electrical energy production in photovoltaic fields under mismatch effect," in *Proceedings of the International Conference on Clean Electrical Power (ICCEP '09)*, pp. 46–51, Capri, Italy, June 2009.

[48] H. Zhu, A. K. Kalkan, J. Hou, and S. J. Fonash, "Applications of AMPS-1D for solar cell simulation," *AIP Conference Proceedings*, vol. 462, pp. 309–314, 1999.

[49] S. Fonash, J. Arch, J. Cuiffi et al. et al., "A manual for AMPS-1D for Windows 95/NT," The Pennsylvania State University, pp. 10–31, 1997.

[50] G. A. M. Hurkx, D. B. M. Klaassen, and M. P. G. Knuvers, "A new recombination model for device simulation including tunneling," *IEEE Transactions on Electron Devices*, vol. 39, no. 2, pp. 331–338, 1992.

[51] K. Yang, J. R. East, and G. I. Haddad, "Numerical modeling of abrupt heterojunctions using a thermionic-field emission boundary condition," *Solid-State Electronics*, vol. 36, no. 3, pp. 321–330, 1993.

[52] Y. Liu, Y. Sun, and A. Rockett, "An improved algorithm for solving equations for intra-band tunneling current in heterojunction solar cells," *Thin Solid Films*, vol. 520, no. 15, pp. 4947–4950, 2012.

[53] https://wiki.engr.illinois.edu/display/solarcellsim.

[54] Y. Liu, Y. Sun, and A. Rockett, "A new simulation software of solar cells—wxAMPS," *Solar Energy Materials and Solar Cells*, vol. 98, pp. 124–128, 2012.

[55] M. Gloeckler, A. L. Fahrenbruch, and J. R. Sites, "Numerical modeling of CIGS and CdTe solar cells: setting the baseline," in *Proceedings of the 3rd World Conference on Photovoltaic Energy Conversion*, vol. 1, pp. 491–494, Osaka, Japan, May 2003.

[56] K. R. McIntosh, J. N. Cotsell, J. S. Cumpston, A. W. Norris, N. E. Powell, and B. M. Ketola, "An optical comparison of silicone and eva encapsulants for conventional silicon PV modules: a ray-tracing study," in *Proceedings of the 34th IEEE Photovoltaic Specialists Conference (PVSC '09)*, pp. 544–549, Philadelphia, Pa, USA, June 2009.

[57] E. E. van Dyk and E. L. Meyer, "Analysis of the effect of parasitic resistances on the performance of photovoltaic modules," *Renewable Energy*, vol. 29, no. 3, pp. 333–344, 2004.

[58] M. A. Green, *Solar Cells: Operating Principles, Technology, and System Applications*, vol. 1 of *Prentice-Hall Series in Solid state Physical Electronics*, Prentice Hall, New York, NY, USA, 1982.

[59] U. Malm and M. Edoff, "Simulating material inhomogeneities and defects in CIGS thin-film solar cells," *Progress in Photovoltaics*, vol. 17, no. 5, pp. 306–314, 2009.

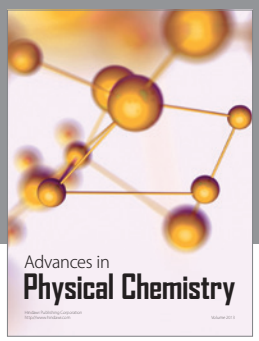

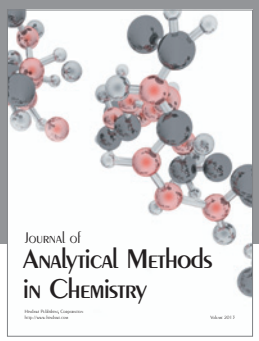

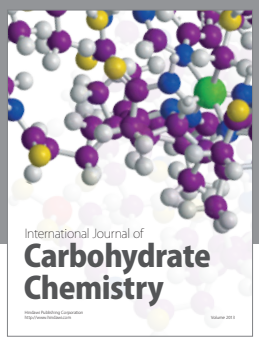

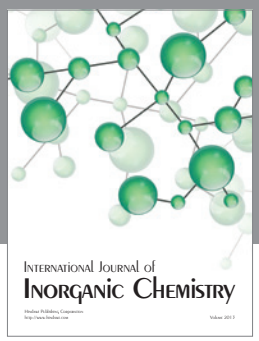

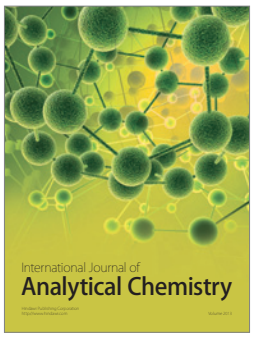

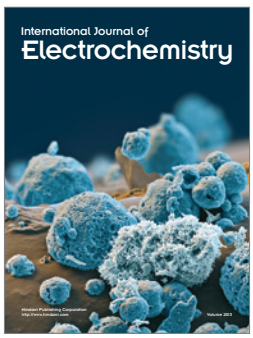

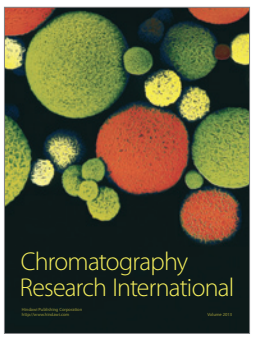

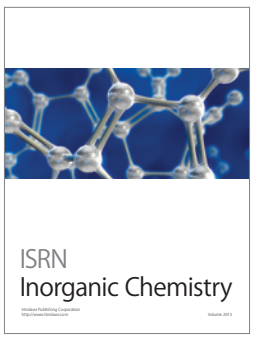

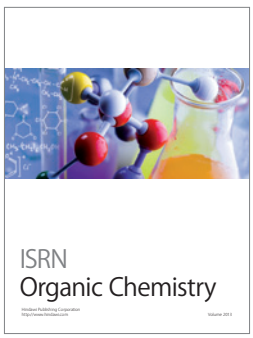

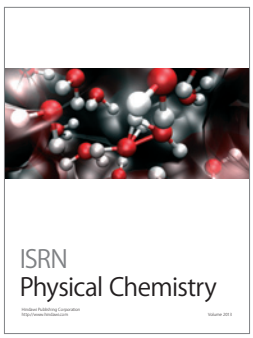

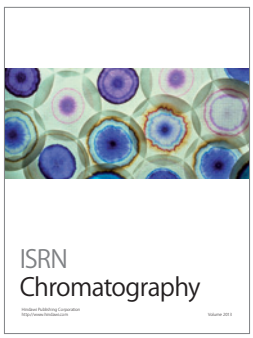

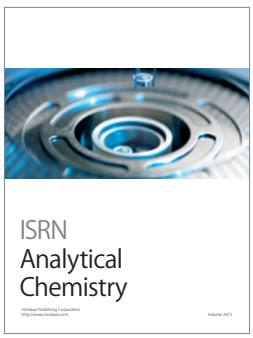

Hindawi

Submit your manuscripts at
http://www.hindawi.com